A Mathematical Model for the Reactive Extrusion of Methyl Methacrylate in a Co-rotating Twin-Screw Extruder

Alejandro Zagal,[†] Eduardo Vivaldo-Lima,*[,‡] and Octavio Manero[†]

Instituto de Investigaciones en Materiales (IIM), Universidad Nacional Autónoma de México (UNAM), Ciudad Universitaria, México D. F., CP 04510, México, and Departamento de Ingeniería Química, Facultad de Química, Universidad Nacional Autónoma de México (UNAM), Conjunto E, Ciudad Universitaria, México D. F., CP 04510, México

A mathematical model for the reactive extrusion of methyl methacrylate (MMA) is presented. Key variables, such as pressure, temperature, residence time, filling ratio, number-average, and weight-average molecular weights (M_n and M_w) along the extruder length can be calculated using the model. The flow in the extruder is modeled using a simplified approach; however, this approach is versatile enough to include any screw profile, such as right-handed and left-handed elements, and kneading disks. A polymerization kinetic model that considers a mixture ("cocktail") of initiators is coupled to the flow equations. An effective model for the auto-acceleration effect is used. Second-order thermal self-initiation of MMA is considered in the reaction mechanism. The model can be easily performed on a personal computer, and a wide range of process conditions can be modeled, because of its flexibility.

Introduction

The use of co-rotating and counter-rotating twin-screw extruders in the polymer-processing, polymer-modifying, and even polymer-producing industries has gained importance lately, because of their versatility and advantages as processing and reaction machines. Although there have been some studies focused on developing quantitative and scientific understanding of the fluid mechanics and transport phenomena that govern the performance of these machines, there is still a need for more studies that are focused on the coupling of fluid mechanics and transport phenomena with polymer reaction engineering, in the case of reactive extrusion in such twin-screw extruders. Janssen[1] has addressed, in depth, the case of counter-rotating twin-screw technology, although the topic is far from being exhausted.

The complexity of the flow in twin-screw extruders, as well as the large number of parameters and interrelated variables that affect the flow, make this process difficult to understand, control, and optimize.

As described by Vergnes et al.,[2] two different approaches concerning the modeling of flow in twin-screw extruders can be distinguished. The first approach uses a local description of the flow field. This approach is very accurate but quite complex. The second approach considers a global description of the entire process, from the feed to the exit section of the extruder, and, consequently, it is a simpler approach.

In the local approach, the first mathematical models that were proposed for flow through the screw elements were one-dimensional (1-D), applicable to both Newtonian and non-Newtonian fluids. Later, two-dimensional (2-D) models for flow along the screw channel, using finite-element methods, were developed. Other 2-D approaches based on the "network-flow analysis method" were conducted by White and co-workers.[3−6] Recently, three-dimensional (3-D) calculations for Newtonian and non-Newtonian fluids have been performed, but only isothermal flows have been considered.

With respect to the co-rotating twin-screw geometry, flow through kneading disks is much more complex than flow along screw channels. However, these flows can be addressed using computational fluid dynamics (CFD) calculations, based on 3-D finite-element simulations. Commercial software packages such as Fluent or Femlab, or institutionally developed and owned codes, can be used to perform such calculations. In the 1980s, some studies on the modeling of flow through screw elements and kneading disks of a modular co-rotating twin-screw extruder, for Newtonian fluids, were published. White and Szydlowski[3] and Meijer and Elemans[7] addressed the problem of modeling starved-flow modular machines. An isothermal, non-Newtonian model was described by Wang et al.[4] Subsequently, composite models including nonisothermal behavior were developed by Chen and White,[8,9] and independently by Potente and co-workers.[10,11] More-recent research studies on the modeling of reactive extrusion in twin-screw extruders have been presented by Berzin and co-workers,[12,13] Fukuoka,[14] Janssen et al.,[15] Gaspar-Cunha et al.,[16] Poulesquen and Vergnes,[17] Gao et al.,[18] and Choulak et al.[19] for different reaction systems and using an ideal plug-flow reactor,[14,18] a series of continuously stirred tank reactors (CSTRs),[19] networks of CSTRs,[14] or CFD-based calculations with commercial or semi-commercial software[16] to model flow within the extruder.

This paper is focused on structuring a mathematical model for the reactive extrusion of methyl methacrylate (MMA) in a modular co-rotating twin-screw extruder. A simplified flow model, first suggested by Vergnes et al.,[2] which includes the equations for the flow in right-handed and left-handed screw elements and kneading disks, is used. The main features of the polymerization

* To whom correspondence should be addressed. Tel.: +(5255)5622-5256. Fax: +(5255)5622-5355. E-mail: vivaldo@servidor.unam.mx.

[†] Instituto de Investigaciones en Materiales (IIM)

[‡] Departamento de Ingeniería Química, Facultad de Química.

10.1021/ie050585b CCC: $30.25
Published on Web 11/05/2005

portion of the model include the use of a mixture of initiators, addressing the auto-acceleration effect with an effective approach, which takes into account the effect of chain length on bimolecular radical termination (using number and weight averages of the termination kinetic rate constant (k_t), requiring no additional model parameters), and including thermal self-initiation of MMA in the reaction mechanism.

Modeling

Flow Equations. It is well-known that the flow along the screws follows an "8"-shaped pattern.[20] It can be visualized as a succession of elements involving flow through C-shaped chambers, and flow through an intermeshing zone between the screws. The flow equations were derived using a cylindrical coordinate system. It was assumed that the flow is locally Newtonian, steady, and isothermal. The radial component of velocity was neglected and inertia is assumed negligible. Therefore, the angular (down-channel velocity) and cross-channel components of velocity are dependent only on position in the radial direction. Using these assumptions and their corresponding boundary conditions, the Stokes equations for the down channel velocity (v) and cross-channel velocity (w) were solved,[21] leading to eqs 1 and 2. The symbols are defined in the nomenclature section.

$$v(r) = \frac{1}{2\eta}\left(\frac{\Delta P}{\Delta\theta}\right)\left[r\left(\frac{R_e^2 \ln(r/R_e) - R_i^2 \ln(\{r\}/\{Ri\})}{R_e^2 - R_i^2}\right) + \frac{1}{r}\left(\frac{R_e^2 R_i^2}{R_e^2 - R_i^2}\right)\ln\left(\frac{R_e}{R_i}\right)\right] + V_e\left(\frac{R_e}{r}\right)\left(\frac{r^2 - R_i^2}{R_e^2 - R_i^2}\right) \quad (1)$$

$$w(r) = \frac{1}{4\eta}\left(\frac{\Delta P}{\Delta z}\right)\left[r^2 - \left(\frac{R_e^2 \ln(r/R_i) - R_i^2 \ln(r/R_e)}{\ln(R_e/R_i)}\right)\right] + \mathrm{We}\left[\frac{\ln(r/R_i)}{\ln(R_e/R_i)}\right] \quad (2)$$

The flow rate through a C-shaped chamber (which is described by eq 3) is obtained on integration of eq 1, with respect to channel length, assuming that the chambers can be modeled as rectangular channels. The cross-channel flow rate is equal to zero. Equation 3 was derived for a right-handed screw element. In a right-handed element, the relative velocity of the barrel has the same direction as the main flow, and the pressure change is generally positive. In contrast, in a left-handed element, the relative velocity of the barrel is opposite to the main flow and has a tendency to drag the fluid upstream. Therefore, to calculate the pressure drop along the C-shaped chamber of a left-handed element, the signs of the two terms of the right-hand side of eq 3 must be changed. Alternatively, the sign of the flow rate can be changed, keeping the right-hand side of eq 3 unchanged.

$$Q_C = F_d W R_e\left[1 - \frac{R_i^2}{R_e^2 - R_i^2}\ln\left(\frac{R_e}{R_i}\right)^2\right]\frac{\Omega R_e}{2}\cos\phi - F_p\left(\frac{1}{8\eta}\right)\left(\frac{\Delta P_C}{\Delta\theta_C}\right)W(R_e^2 - R_i^2)\left\{1 - \left[\frac{2R_iR_e}{R_e^2 - R_i^2}\ln\left(\frac{R_e}{R_i}\right)\right]^2\right\} \quad (3)$$

It is interesting to note that eq 3 may be used to calculate the flow along partially filled right-handed screw elements, if ΔP_C is made equal to zero, and W is replaced with the filled width of the channel, W'. The specific flow behavior used in this paper ensures that the left-handed screw elements are always fully filled.

The geometry and kinematics in the intermeshing zone have been studied by Tayeb et al.,[22] using a simple model in which the relative displacement of the screws is neglected and a pressure flow is assumed. In the model used in this paper, an approximate mean cross section, which is defined from the main characteristic parameters of the screw and barrel geometry, is used. The width of this area is calculated using eq 4.[22] The parameter α in eq 4 is the tip angle defined by Booy,[23] who made a detailed analysis of the geometry of twin-screw extruders.

$$W^* = W - \alpha R_e \sin\phi \quad (4)$$

When the staggering angle is greater than the tip angle (α), in a block of kneading disks, a gap opens between adjacent channels, leading to a leakage flow (Q_L) that is associated with flow recirculation and distributive mixing. The two other flows are the channel flow (Q_C) and the overflight flow (Q_f). Q_f does not contribute to the extruder output; therefore, it was neglected in the calculations.

The flow in the kneading disks is similar to that in the right-handed screw elements. The flow in kneading disks is very complex; therefore, a simplified approach that has been used by Della Valle et al.[24] is briefly described here. An equivalent geometry is defined for a block of kneading disks to simplify the calculations. The equivalent pitch for the block of kneading disks (B_e) is defined in eq 5.

$$B_e = \frac{2\pi}{\Delta\theta_l}e \quad (5)$$

The available section for flow is approximated by a rectangular channel of width W_e, length L_e, and depth h_e; $\Delta\theta_l$ is the staggering angle between two adjacent kneading disks, and e is the disk thickness. It is very important to note that the equivalent geometry is correctly defined only if small staggering angles are used; therefore, angles of 90° are inappropriate. After the equivalent pitch has been defined, expressions for the equivalent angle, the equivalent width, and the equivalent depth are readily obtained. The results are shown in eqs 6, 7, and 8, respectively.

$$\phi_e = \tan^{-1}\left(\frac{e}{\Delta\theta_l R_e}\right) \quad (6)$$

$$W_e = \frac{B_e\cos\phi_e}{m} - e \quad (7)$$

$$h_e = R_e\left[1 + \cos\left(\frac{\Delta\theta_l}{2}\right)\right] - \sqrt{C_L^2 - R_e^2\sin^2\left(\frac{\Delta\theta_l}{2}\right)} \quad (8)$$

To calculate Q_L, an equivalent geometry that is similar to that defined for Q_C is used. Equations 5−8 can be used, if the angle $\Delta\theta_l$ is substituted by $\pi - \Delta\theta_l$. The total outlet flow from a block of kneading disks is the contribution from a C-shaped chamber (Q_C) and the transversal flow through the gap between the disk tips (Q_L). The leakage flow Q_L is calculated using eq 9,

provided that the velocity component perpendicular to the continuous channel (v_l) is known.

$$Q_L = -\frac{F_{pl}}{12\eta}\left(\frac{\Delta P_l}{L_{el}}\right)W_{el}h_{el}^{\ 3} + F_{pl}W_{el}\left(\frac{v_l}{2}\right)h_{el} \qquad (9)$$

F_{pl} and F_{dl} in eq 9 are shape factors for the leakage flow. The pressure drop along the gap is given by eq 10, where $\Delta\theta_l$ is the kneading disk staggering angle and $dP_C/d\theta$ is the angular pressure drop along the continuous channel, which is calculated using eq 3.

$$\frac{\Delta P_l}{L_{el}} = \frac{dP_C}{d\theta}\Delta\theta_l \qquad (10)$$

Rheology. The rheological properties of the system change drastically when methyl methacrylate (MMA) is polymerized to poly(methyl methacrylate) (PMMA). The rheology of a mixture of MMA and PMMA is strongly affected by composition (conversion, in a reacting system), which determine the molecular weight, and other variables, such as temperature and shear rate. Stuber[25] correlated the rheological variables of a solution of MMA and PMMA with the polymer concentration, weight-average molecular weight, temperature, and shear rate.

To make a complete characterization of the dependence of viscosity of a solution of MMA/PMMA on shear rate, it is necessary to know the power-law constant of the system, and the moment when the transition from Newtonian to non-Newtonian behavior occurs. To model the evolution of viscosity in a reactive extruder, the zero-shear viscosity and the high-shear-rate power-law dependence must be combined into a single expression. The Ellis model combines both ranges of shear-rate dependence, as shown in eq 11, where η_0 is zero-shear viscosity, n the power-law constant, m' the Ellis constant, $\dot\gamma$ the shear rate, and η the viscosity.

$$\eta(\dot\gamma) = \frac{\eta_0}{1 + m'\dot\gamma^{1-n}} \qquad (11)$$

The parameters in eq 11 are functions of temperature, molecular weight, and polymer concentration, as proposed by Stuber,[25] and are described in eqs 12−16,

$$m'(c,M,T) = \frac{0.0140616(n-1)M^{0.5}c^4}{T^3} \qquad (12)$$

$$n(c,M,T) = \exp\left(\frac{-13.8155M^{0.5}c^4}{T}\right) \qquad (13)$$

$$\eta_0(c,M,T) = F\zeta \qquad (14)$$

$$F = K[1 + a_1(cM)^{0.5} + a_2(cM)^{3.4}] \qquad (15)$$

$$\zeta = \exp\left[(b_0 + b_1c + b_2c^2)\left(\frac{1}{T} - \frac{1}{T_{ref}}\right) + b_3c^3\right] \qquad (16)$$

where c is the polymer concentration (weight percent), M the polymer molecular weight (in thousands), and T the temperature (in Kelvin). The symbols K, a_1, a_2, b_0, b_1, b_2, and b_3 represent constants that have been adjusted by Stuber[25] and are given in Table 1.

The shear rate is calculated using eq 17, where v and w are given by eqs 1 and 2, respectively. In eqs 1 and 2, the Newtonian viscosity is replaced by the shear-rate-dependent viscosity (see eq 11). The resulting expressions result in an approximated power-law flow model. The radial velocity is neglected, and it is assumed that the angular and axial velocities are dependent only on the radial position.

Table 1. Parameters for Calculation of Zero-Shear Viscosity

parameter	value
K	2.16×10^{-4} Pa s
a_1	0.125
a_2	3.75×10^{-11}
b_0	600
b_1	80
b_2	1
b_3	1.2×10^{-5}
T_{ref}	465.15 K

$$\dot\gamma = \frac{2}{R_e^{\ 2} - R_i^{\ 2}}\int_{R_e}^{R_i} r\left[\left(\frac{dv}{dr} - \frac{v}{r}\right)^2 + \left(\frac{dw}{dr}\right)^2\right]^{1/2} dr \qquad (17)$$

Polymerization Kinetics. The reaction scheme for conventional free-radical polymerization in the presence of a mixture of five initiators, and considering monomer thermal self-initiation, as used in this paper, is shown in Table 2.

The equations that describe the polymerization kinetics and molecular weight development in free-radical polymerization systems are well-known (e.g., Vivaldo-Lima et al.[26]). Equations 18−25 show the equations that model the system represented by the reaction mechanism shown above. Molecular weight development is represented in terms of the moments of the molecular weight distribution. The moment equations (eqs 20−25) are obtained through application of the well-known method of moments to the detailed polymer material balance equations.

$$R_I = -\sum_{i=1}^{5} k_{di}I_i \qquad (18a)$$

$$I = \sum_{i=1}^{5} I_i \qquad (18b)$$

$$R_M = R_p = -k_{it}M^2 - k_pM\lambda_0 \qquad (19)$$

$$R_{\lambda_0} = 2\sum_{i=1}^{5} f_i k_{di}I_i + k_{it}M^2 - (k_{tc} + k_{td})\lambda_0^{\ 2} \qquad (20)$$

$$R_{\lambda_1} = 2\sum_{i=1}^{5} f_i k_{di}I_i + k_{it}M^2 + k_pM\lambda_0 - (k_{tc} + k_{td})\lambda_1\lambda_0 \qquad (21)$$

$$R_{\lambda_2} = 2\sum_{i=1}^{5} f_i k_{di}I_i + k_{it}M^2 + k_pM(\lambda_0 + 2\lambda_1) - (k_{tc} + k_{td})\lambda_2\lambda_0 \qquad (22)$$

$$R_{\mu 0} = \left(\frac{k_{tc}}{2} + k_{td}\right)\lambda_0^{\ 2} \qquad (23)$$

$$R_{\mu_1} = (k_{tc} + k_{td})\lambda_0\lambda_1 \qquad (24)$$

$$R_{\mu_2} = k_{tc}(\lambda_0\lambda_2 + \lambda_1^{\ 2}) + k_{td}\lambda_0\lambda_2 \qquad (25)$$

Auto-Acceleration Effect. A comparative study on the performance of the Marten−Hamielec[27] (MH) and

Table 2. Reaction Scheme

chemical initiation	$I_1 \xrightarrow{k_{d1}} 2R^*$
	$I_2 \xrightarrow{k_{d2}} 2R^*$
	$I_3 \xrightarrow{k_{d3}} 2R^*$
	$I_4 \xrightarrow{k_{d4}} 2R^*$
	$I_5 \xrightarrow{k_{d5}} 2R^*$
thermal self-initiation	$2M \xrightarrow{k_{it}} 2R^*$
first propagation step	$R^* + M \xrightarrow{k_i} P_1^*$
propagation	$P_n^* + M \xrightarrow{k_p} P_{n+1}^*$
termination by combination	$P_n^* + P_m^* \xrightarrow{k_{tc}} D_{n+m}$
termination by disproportionation	$P_n^* + P_m^* \xrightarrow{k_{td}} D_n + D_m$

Chiu−Carratt−Soong[28] (CCS) models was performed by Vivaldo-Lima et al.[26] The purpose of that study was to develop an accurate and simple model for diffusion-controlled phenomena in free-radical polymerization, which is the one that has been used in this paper. The main features of the model proposed therein include having a simple structure, reliability of predictions (because of its sound theoretical background), and robust parameter estimates. Equations 26−30 summarize the model equations for diffusion-controlled phenomena.

$$k_p = k_{p_0} \exp\left[B\left(\frac{1}{Vf} - \frac{1}{Vf_{cr2}}\right)\right] \tag{26}$$

$$k_{tn} = k_{t_0} \exp\left[-A\left(\frac{1}{Vf} - \frac{1}{Vf_0}\right)\right] \tag{27}$$

$$k_{tw} = k_{t_0}\sqrt{\left(\frac{\overline{P_n}}{\overline{P_w}}\right)^X} \exp\left[-A\left(\frac{1}{Vf} - \frac{1}{Vf_0}\right)\right] \tag{28}$$

$$f = f_0 \exp\left[-D\left(\frac{1}{Vf} - \frac{1}{Vf_0}\right)\right] \tag{29}$$

$$v_f = \sum_{i=1}^{\text{number of components}} [0.025 + \alpha_i(T - T_{gi})]\frac{V_i}{V_t} \tag{30}$$

The use of a single k_t in modeling free-radical polymerizations would be valid if the termination reactions were independent of chain length. The use of k_t average values to calculate the polymerization rate, as well as the weight-average and number-average molecular weights, was suggested elsewhere.[29] The statistical averages of k_t have been obtained from data on the conversion and molecular weight averages. A simpler and effective way to calculate the k_t averages was suggested by Vivaldo-Lima et al.[26] Equations 27 and 28 define the number-average and weight-average values of k_t,[26] respectively. Equation 27 is used to calculate the zeroth and first moments of the live and dead polymer population, whereas the second moment of the live and dead polymer populations is calculated using k_t from eq 28. The fractional free volume (v_f) is calculated using eq 30. The symbol v_{f0} represents the free volume under the initial conditions.

Energy Balance. Twin-screw extrusion processes are highly nonisothermal. Therefore, the calculation of temperature profiles is very important. In this paper, only variation of the main temperature over the channel depth is being considered. In the former sections (those containing screw elements and kneading disks), isothermal equations for small sub-elements (C-shaped chambers) are used. The energy balance from one sub-element to another is shown in eqs 31 and 32,

$$\rho C_p Q_C \frac{dT}{d\theta} = \frac{dQ_{tot}}{d\theta} \tag{31}$$

$$\rho C_p Q_C \, dT = h_{T_b}(T_b - T)S_b + h_{T_s}(T_s - T)S_s + \dot{W} + Q_C H_p \, dM \tag{32}$$

where C_p is the specific heat capacity; h_{T_b} and h_{T_s} are barrel and screw heat-transfer coefficients, respectively; S_b and S_s are exchange surfaces; $\dot{W}$ is the dissipated power; H_p is the reaction enthalpy; and dM is the change in monomer concentration. Equation 31 comes from a macroscopic energy balance applied in differential form along the flow trajectory. This equation tells us that the energy gained by the fluid along the flow trajectory is equal to the total heat transferred to the system by the surroundings and the heat generated by the chemical reaction and viscous dissipation. The energy balance equation is coupled to the flow through the heat-transfer coefficients and the viscous dissipation term, because these terms involve the viscosity and shear rate, respectively. Conversely, the viscosity itself is dependent on temperature through eqs 11−16. This leads to eq 32, where the barrel heat-transfer coefficient is given by eq 33. This coefficient was determined experimentally by Todd.[30]

$$h_{T_b} = 0.69\frac{k}{Re}\left(\frac{Re^2 N\rho}{\eta(\dot{\gamma})}\right)^{0.28}\left(\frac{C_p\eta(\dot{\gamma})}{k}\right)^{0.33}\left(\frac{\eta(\dot{\gamma})}{\eta_p(\dot{\gamma})}\right)^{0.14} \tag{33}$$

In eq 32, $\eta(\dot{\gamma})$ and $\eta_p(\dot{\gamma})$ are the bulk viscosity and viscosity at the wall, respectively. A similar expression is given for the screw heat-transfer coefficient.

The dissipated power in a sub-element is calculated by integration over the volume of the sub-element, as shown in eq 34. Temperature for the different sub-elements is calculated using eqs 31−33 and 35.

$$\dot{W} = \int_V \eta\dot{\gamma}^2 \, dV \tag{34}$$

$$T_{i+1} = T_i + \Delta T_i \tag{35}$$

Overall Reactive Extrusion (REX) Model. In the previous sections, equations for different aspects of reaction extrusion have been described. The next step is to link all these equations, to obtain a global model, which should be capable of describing the complete process correctly.

The chambers in the screw of an extruder can be partially filled, or fully filled. For fully filled sub-elements, the mean residence time is defined as shown in eq 36,

$$t_s = \frac{V}{Q_C} \tag{36}$$

where V is the available volume of the sub-element. In partially filled sub-elements, the reaction mixture is conveyed through the extruder by pure drag flow. Therefore, the mean residence time for an axial

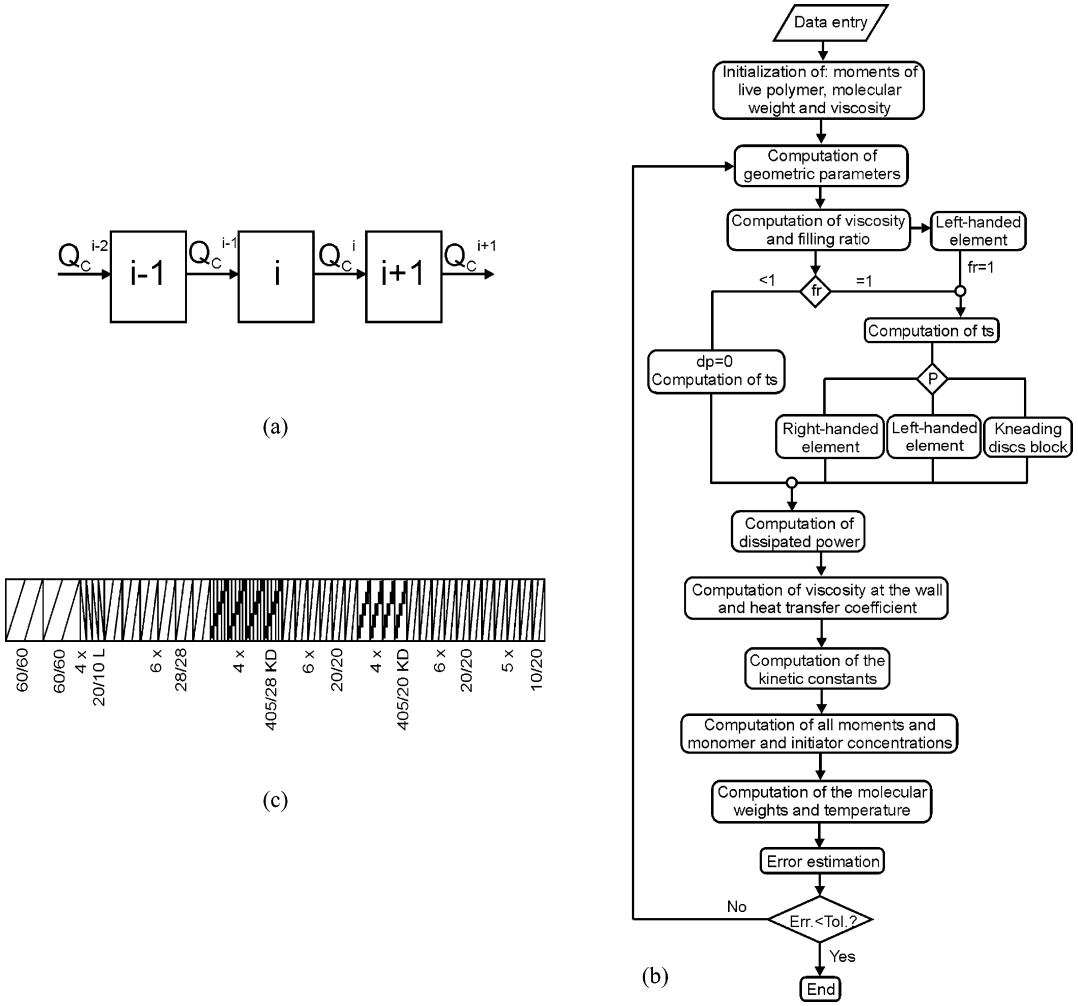

Figure 1. Some aspects of the modeling approach: (a) connections among the series of reactors inside the extruder; (b) flow diagram of the calculation sequence; and (c) screw profile.

length L is given by eq 37,

$$t_s = \frac{L}{\bar{V}\sin\phi} \tag{37}$$

where L is the axial length of the sub-element and $\bar{V}$ is the mean velocity along the channel direction.

The filling ratio is defined as the ratio of the volume occupied by the polymer blend to the free volume available in the sub-element, as shown in eq 38,

$$f_r = \frac{2Q_C L}{NVB\cos^2\phi} \tag{38}$$

where N is the rotational speed of the screw (given in terms of the number of turns per second) and B is the screw pitch.

The viscosity calculation is performed using eqs 11−17. Equation 17 requires the derivatives of the velocity components, which are obtained from eqs 1 and 2. The shear rate for each chamber is calculated using eq 17. The mean shear rate is calculated by integration of eq 17 along the channel depth.

Calculation of the pressure drop involves the values of the pressure drop along the gap, and the angular pressure gradient, given in eqs 3 and 10, respectively. Q_L is calculated using eq 9, and a new flow rate is estimated with $Q_C^* = Q_C - Q_L$. With this new flow rate, the calculation is repeated for the following element, up to the total number of elements (disks). Finally, summation of the angular pressure gradients for each element is performed to obtain the total pressure increase along the extruder.

In co-rotating twin-screw extruders with small gaps, leakage flows among channels are very small, compared to the main flow, as opposed to the case of counter-rotating twin-screw extruders with similar gaps. The magnitudes of the main and leakage flows were evaluated from eqs 3 and 9, respectively. To calculate the leakage flow, the pressure drop along the gap (eq 10) was used. Because this flow is usually a small fraction of the main flow, the total outlet flow coming from one sub-element is assumed to be the same as the inlet flow into the next sub-element. Each sub-element is assumed to behave as a small continuous stirred tank reactor (CSTR). The connections among the different CSTRs that model the flow in the extruder are shown in Figure 1a. The volume of each CSTR is dependent on whether the chambers are fully or partially filled. The volume of fully filled chambers can be calculated using eq 39.[23]

$$V = \frac{L}{3}\Big([2(\pi-\psi)R_e^2 + C_L R_e \sin\psi] - 2\Big\{m(\psi C_L^2 - C_L R_e \sin\psi) + \frac{1}{2}m\alpha[R_e^2 + (C_L - R_e)^2]\Big\}\Big) \tag{39}$$

For partially filled chambers, the corresponding volume is determined by the axial length of the sub-element, the mean velocity, and the screw pitch angle, as shown in eq 37.

The material balance around the ith reactor, assuming equal inlet and outlet flows, is given by eq 40,

$$x^{i-1} = x^i - t_s{}^i R_{x^i} \tag{40}$$

where x^i represents the mass of species x in the ith chamber. From eqs 18 and 40, the initiator concentration at chamber i of the extruder can be obtained, as indicated in eq 41.

$$I_k^i = \frac{I_k^{i-1}}{1 + t_s^i k_{dk}} \qquad (k = 1, 2, ..., 5) \tag{41}$$

From eqs 19, 20, and 40, the monomer and total polymer radical concentrations can be calculated, leading to eqs 42 and 43.

$$4k_{it}(M^i)^2 + M^i\left(\frac{1}{t_s^i} + k_p\lambda_0^i\right) - \frac{M^{i-1}}{t_s^i} + 2\sum_{k=1}^{5} f_k k_{dk} I_k = 0 \tag{42}$$

$$k_t(\lambda_0^i)^2 + \frac{\lambda_0^i}{t_s^i} - 2\sum_{k=1}^{5} f_k k_{dk} I_k - 2k_{it}(M^i)^2 - \frac{\lambda_0^{i-1}}{t_s^i} = 0 \tag{43}$$

Equation 42 can be analytically solved for M^i, which, upon substitution into eq 43, allows calculation of the zeroth moment (total polymer radical concentration) of the polymer radical population. After this polymer radical concentration is known, using the Newton−Raphson method (eq 44), the monomer concentration can be obtained from the analytical solution of eq 42.

$$(\lambda_0^i)_{k+1} = (\lambda_0^i)_k - \frac{f[(\lambda_0^i)_k]}{f'[(\lambda_0^i)_k]} \tag{44}$$

The function involved in the Newton−Raphson method for the zeroth moment of the polymer radical population can be expressed as shown in eq 45.

$$f[(\lambda_0^i)_k] = k_t(\lambda_0^i)^2 + \frac{\lambda_0^i}{t_s^i} - 2\sum_{k=1}^{5} f_k k_{dk} I_k - \frac{\lambda_0^i}{t_s^i} - 2k_{it}\left[\frac{M^{i-1} + 2t_s^i\sum_{k=1}^{5} f_k k_{dk} I_k - 2t_s^i k_t(\lambda_0^i)^2 - 2\lambda_0^i + 2\lambda_0^{i-1}}{1 + k_p t_s^i \lambda_0^i}\right]^2 \tag{45}$$

The same procedure is followed for the remaining moments to calculate the concentrations of all the species in the ith chamber. Number- and weight-average molecular weights are calculated as ratios of moments of the molecular weight distribution, as shown in eqs 46 and 47.

$$\bar{M}_n = \frac{\lambda_1 + \mu_1}{\lambda_0 + \mu_0} M_0 \tag{46}$$

$$\bar{M}_w = \frac{\lambda_2 + \mu_2}{\lambda_1 + \mu_1} M_0 \tag{47}$$

The moments of the molecular weight distribution are treated as species. Therefore, they are calculated using eqs 20−25 and 40.

The variables used in this model are inter-related; therefore, it is necessary to use iterative procedures to solve the equations. The calculation sequence used to solve the global model is shown in Figure 1b. First, an initial estimate of the moments and molecular weight averages are required. These were estimated by setting the time derivatives of the zeroth, first, and second moments to zero, which resulted in a first estimate of the weight-average molecular weight. With the initial data of molecular weight, temperature, and composition, the viscosity of the reacting mixture is calculated using eq 11, and, subsequently, the velocity components are calculated using eqs 1 and 2. The value of the pressure drop in the ith chamber requires information on the filling ratio. Because the feed to the extruder is either a monomer or a pre-polymerized mixture of MMA (not a solid), and given the fact that the feed flow rate is known, the filling ratio can be calculated at any stage along the flow trajectory. If the filling ratio is <1, the pressure drop is equal to zero and the residence time is calculated using eq 36, corresponding to partially filled sub-elements. If the filling factor is equal to 1 and corresponds to a right-handed screw element, the pressure drop is calculated using eq 3 and, for the kneading disks, eqs 9 and 10 are used. For a left-handed element, the filling factor is set equal to 1 and the pressure drop is calculated using eq 3. For all cases when the filling factor is 1, the residence time is given by eq 36.

The viscous dissipation term (eq 34) is evaluated upon calculation of the shear rate and viscosity, through eqs 11 and 12. The heat-transfer coefficients are also calculated from the value of the viscosity at the wall and in the core, respectively. Hence, the energy balance (eq 32) provides an updated temperature for each element.

The kinetic block of the solution chart is initiated from the evaluation of the kinetic rate constants from eqs 26−30. Parameters such as X (monomer conversion), $\overline{P_n}$, and $\overline{P_w}$ (the number- and weight-average chain lengths, respectively) are initialized using the value obtained from the previous chamber and are updated at every iteration. Subsequently, the compositions of the five initiators are calculated (eqs 18 and 40), and the monomer concentration and the zero moment are solved using eqs 19, 20, and 40, using the Newton−Raphson iterating technique. Thereafter, the remaining moments are calculated through eqs 2−25 and the number- and weight-average molecular weights by eqs 41 and 42. With the updated values of the average molecular weights, compositions, and temperature, the shear rate and viscosity are once again evaluated at every radial position. The energy balance provides a new temperature and the iteration cycle is repeated. Iterations are performed until the values of the variables between two

Table 3. Summary of Model Parameters Used in Simulations

parameter	value	reference	remarks
A	1.45 ± 0.407	34	diffusion-controlled effects
B	0.7 ± 0.22	34	diffusion-controlled effects
D	10^{-3}	34	diffusion-controlled effects
V_{fcr2}	$\exp(-8.39-639/T)$	34	temperature (T) given in Kelvin
k	0.25 W mol^{-1} K^{-1}	35	thermal conductivity
k_{d1}	$2.89 \times 10^{15} \exp(-15664/T)$ s^{-1}	36	Perkadox AIBN
k_{d2}	$4.12 \times 10^{15} \exp(-15366/T)$ s^{-1}	36	Trigonox 125
k_{d3}	$1.77 \times 10^{15} \exp(-15890/T)$ s^{-1}	36	Trigonox 121
k_{d4}	$2.22 \times 10^{16} \exp(-17850/T)$ s^{-1}	36	Trigonox 131
k_{d5}	$4.02 \times 10^{15} \exp(-17843/T)$ s^{-1}	36	Trigonox 201
k_{it}	$6.19 \exp(-9098/T)$ L mol^{-1} s^{-1}	37	
k_{p0}	$2.67 \times 10^{6} \exp(-2689.3/T)$ L mol^{-1} s^{-1}	38	
k_{td}/k_{tc}	$2483 \exp(-2050/T)$	39	
k_{t0}	$4.76 \times 10^{7} \exp(-267/T)$ L mol^{-1} s^{-1}	40	
T_{gm}	167 K	34	monomer
T_{gp}	378 K	35	polymer
C_p	2.3 kJ kg^{-1} K^{-1}	35	
α_m	0.001 K^{-1}	34	monomer
α_p	0.00048 K^{-1}	35	polymer
ρ_m	$0.9659 - 0.0001213T$ kg/L	35	monomer; temperature (T) given in Celsius
ρ_p	$1.2 - 0.000481T$ kg/L	35	polymer; temperature (T) given in Celsius
H_p	−57.8 kJ/mol	35	

Table 4. Process Conditions

parameter	value
feed temperature, T_0	70 °C
barrel temperature, T_b	
zone 1	110 °C
zone 2	120 °C
zone 3	140 °C
zone 4	120 °C
zone 5	120 °C
zone 6	120 °C
feed flow, Q_0	22.08 L/s (350 gal/min)
screw speed	10.47 rad/s (100 rpm)
feed conversion, X_0	10

successive runs agree, to some predetermined tolerance level. These iterative cycles render results for the first chamber, and the process continues until all chambers of the extruder are completed.

Conceptually, our approach is similar to that reported by Keum and White,[31] in the sense that they coupled a fluid mechanics model[32,33] in a backward direction, which was coupled to an energy balance that was calculated in a forward direction, and a kinetic model (using the method of moments, but for the grafting of polyethylene).

Results and Discussion

Reference System. The dimensions of a Werner & Pfleiderer ZSK30 extruder were used in the simulations presented in this paper. The screw diameter was 30 mm, and the shaft length was 871 mm. The screw profile is shown in Figure 1c. An overall initiator initial concentration of 0.3 wt % was used, consisting of 60% Trigonox 125 (*tert*-Amyl peroxypivalate, $f = 0.75$), which reaches its half-life in 0.1 h at 91 °C, and 40% of Trigonox 201 (di-*tert*-amyl peroxide, $f = 0.85$), which reaches its half-life in 0.1 h at 150 °C. The model parameters and process conditions used in the calculations presented in this paper are summarized in Tables 3 and 4, respectively.

Comparison of Calculation Procedures To Model the Extruder ("Hopper to Die" versus "Die to Hopper" Approaches). The calculation procedure to model the extruder described in the modeling section of this paper goes from hopper to die ("forward" approach). It has been argued in the literature that the calculation should be carried backward, namely, from die to hopper.[12,13] Our calculation strategy, which has been described previously, was modified to allow backward calculations. One of the most difficult issues to address when implementing the backward approach is to define the initial conditions properly. To address this issue, several strategies were attempted, including establishing bounds to the values of the calculated variables, using the solution of an isothermal forward calculation as an initial solution, and finally, and what turned out to be most effective, to use the solution of the same problem, obtained with the forward algorithm, as an initial condition.

Figure 2a shows model predictions of the number-average molecular weight versus conversion along the extruder length. In addition, predictions of the conversion (Figure 2b), viscosity (Figure 2c), and melt temperature at the centerline (Figure 2d), versus extruder length, are illustrated. The pressure along the extruder length is almost constant (2 bar), and, for this reason, it is not shown. In these cases, the results shown include both the forward (hopper to die) and backward (die to hopper) calculation approaches. As observed, the agreement is complete, because the profiles overlap for all variables considered.

In Figure 2d, the model predictions show that the centerline temperature increases from 70 °C to 180 °C, from the beginning to the full length of the extruder. It is also observed that the temperature of the melt is higher than the barrel temperature along the last 20% of the extruder length, next to the die. This is the region where significant viscous dissipation occurs, which coincides with the sudden upturn in conversion, as shown in Figure 2a, and with the more gradual upturn in the viscosity (Figure 2c). However, one should remember that the melt temperature calculated from the energy balance equation strictly corresponds to the temperature at the centerline of the extruder cylinder. The temperature between the centerline of the outer cylinder and the wall may vary between those two values. These high-temperature values inside the extruder cause a decrease in the number-average molecular weight, the values of which fall too short of the

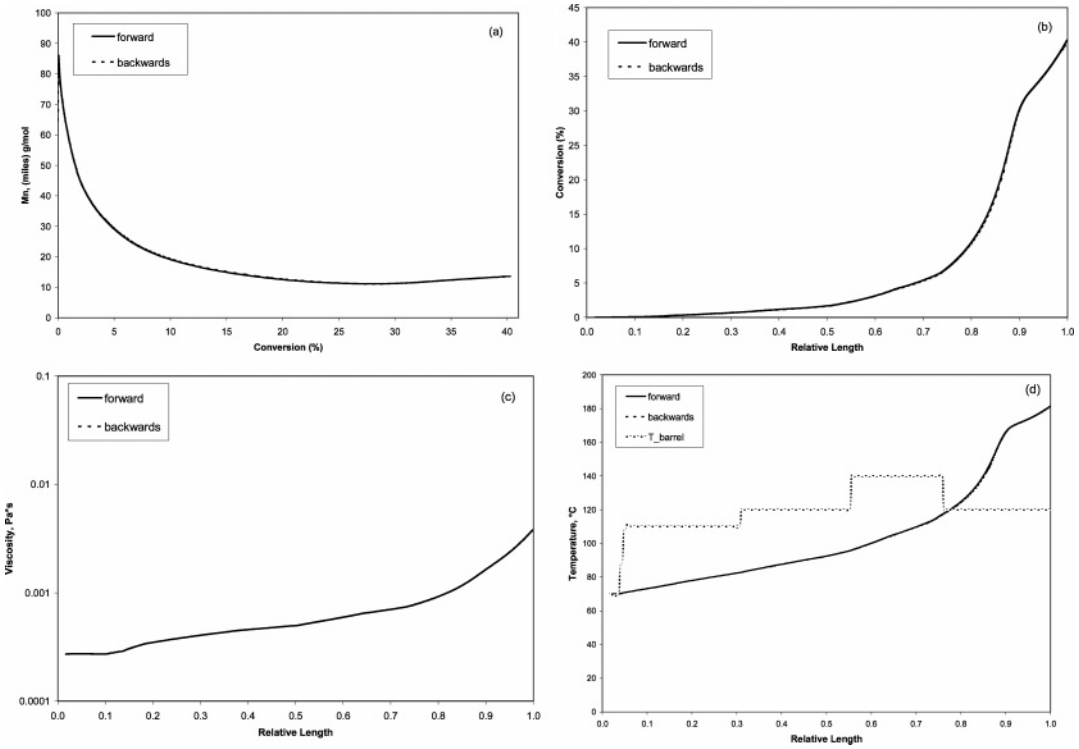

Figure 2. Comparison of forward and backward modeling approaches, for the following profiles: (a) number-average molecular weight versus monomer conversion, (b) conversion versus fractional extruder length, (c) viscosity versus fractional extruder length, and (d) melt and barrel temperatures versus extruder relative length.

commercial value range. The predictions of number- and weight-average molecular weights at high temperatures (above ~140 °C) may not be accurate enough, because the depropagation reaction, which is important at high temperatures, was neglected in our model. The inclusion of depropagation might lead to even lower molecular weights. However, the predictions at high temperatures are also uncertain, because the kinetic rate constants used in the model calculations were not evaluated at such high-temperature ranges.

The dependence of viscosity on molecular weight, polymer concentration, and temperature is expressed in eqs 11−17. As observed, the zero-shear viscosity is a strong function of polymer concentration, so any decrease in molecular weight is offset by the corresponding increase in polymer concentration, or by high monomer conversion. In summary, it should be considered that viscosity is determined not only by polymer molecular weight, but also by polymer concentration. At the beginning of the polymerization (short lengths of the extruder), the molecular weight is high, but the polymer concentration is low, thus producing rather low viscosity values. As polymerization proceeds, even when the molecular weight is decreased because of the increasing temperature profile, the viscosity continues to gradually increase, because of the increase in polymer concentration.

Effect of Process Variables. Simulations using the model, and comparison of experimental data from Balke and Hamielec[41] for batch reactors with isothermal model predictions using the equations of an extruder with residence time as independent variable, are shown in this section.

A plot of global conversion versus fractional extruder length for different feed conversions is presented in Figure 3. As observed, the final conversion is strongly dependent on the feed characteristic conversion. Overall,

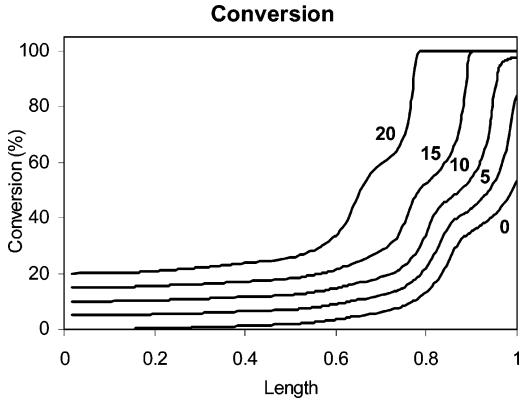

Figure 3. Effect of feed conversion on global conversion within the extruder (feed conversions: 0%, 5%, 10%, 15%, and 20%).

by increasing the feed conversion to values larger than 5%, final conversions close to 100% are obtained. These can be reached at increasing distances from the die. For example, when the feed conversion is 20%, the final conversion of 100% is obtained during the first 70% of the extruder length. The temperature profile along the extruder for the different feed conversions is shown in Figure 4. As observed, three of the curves reach a temperature of ~270 °C near the die. This prediction is substantiated by the evolution of the heat of polymerization, and the effect of viscous dissipation, which becomes important at the final stages of the process where the conversion is high. It is also observed that the sharp increase in conversion, in all cases shown in Figure 3, which can be associated to a strong autoacceleration effect, typical of MMA polymerization, is accompanied by a huge increase in temperature. This means that the heat-removal efficiency is very low.

Figure 5 shows the concentration profiles of the two initiators used in the reference case simulations under

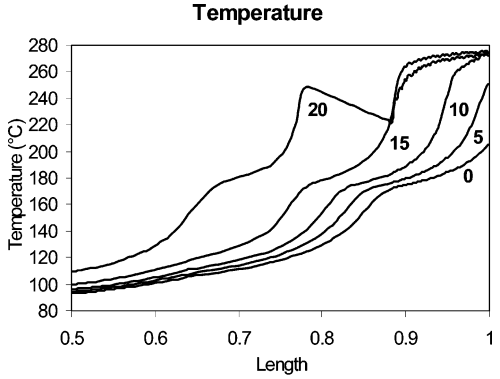

Figure 4. Temperature versus fractional extruder length for various feed conversions (0%, 5%, 10%, 15%, and 20%).

the conditions of Table 4. Their concentrations remain almost constant during most of the extruder length, up to certain temperature values (depending on the half-life time of the initiators) where their decomposition rates becomes fast, and, because the temperature continues to increase to very high values, the concentration of the initiators falls rapidly to zero. Trigonox 125 is completely consumed at ~83% of the extruder relative length, and Trigonox 201 is completely consumed at 97% of the extruder relative length. This observation means that the chosen initiators were adequate for the given process conditions. If the temperature was constant, or if it did not reach such high values as those observed in Figure 4, the chosen initiators would have been inadequate, because they would have not been consumed to significant levels, given the low values of their decomposition kinetic rate constants, at temperatures that were not very high.

Predictions of the number-average molecular weight M_n versus fractional extruder length are shown in Figures 6 and 7, for several feed and barrel temperatures, respectively. An interesting effect on the development of the molecular weight profile is predicted by the model, i.e., the drastic decrease of almost a decade in molecular mass along the extruder length. The decrease is continuous and tends toward a common value, near the die. The number-average molecular weight decreases with length, because the reaction mixture temperature increases considerably, which, in the early stages of the polymerization, is strongly dependent on the feed temperature and, in the latter stages, is dependent, to some extent, on the barrel temperature. The temperature of the reaction mixture is strongly determined by the heat of reaction from the middle stages to the final stages of polymerization.

Figure 8 shows predictions of viscosity versus fractional or relative length, from hopper to die, for different feed volumetric flow rates. The larger the flow rate, the shorter the residence time and the lower the conversions that are obtained, and vice versa. Therefore, high reaction-mixture viscosity values are reached with the smallest feed flow rate. An increase in residence time caused by variation of the flow rate results in a higher conversion, which strongly affects the reaction-mixture viscosity. On the other hand, in Figure 9 (viscosity versus fractional extruder length for several screw speeds), the viscosities predicted by the model are less than those of Figure 8. In Figure 9, only one of the curves reaches a value of 10 Pa s, whereas, in Figure 8, viscosities of >100 Pa s are obtained. The viscosity values plotted in Figures 8 and 9 are substantially low, because of the high temperature that is attained by the reaction mixture. Once again, it is observed that the viscosity along the extruder length is increased when the number-average molecular weight is decreased. As explained in the previous subsection, this apparently inconsistent result may be caused by the viscosity increase promoted by the increase in polymer concentration. In Figure 8, the viscosity increases steadily in only one curve (that assigned to the lower mass rate). The remaining curves show an asymptotic behavior. In Figure 9, at low rotational speeds, viscosity indeed decreases after a maximum, which indicates the dominating effect of low molecular weight and high temperature at the immediate proximity of the die. For larger rotational speeds, the asymptotic behavior of viscosity indicates a balance between the temperature (which decreases viscosity) and concentration (which increases viscosity) effects. Overall, the asymptotic viscosity magnitudes in Figures 8 and 9 are still small.

If the temperature is kept constant along the extruder length, and residence time is used as the independent variable, the behavior of the extruder would be equivalent to that of a batch reactor. To test the correct implementation of the polymerization kinetic model, a comparison of experimental data by Balke and Hamielec[41] for free-radical polymerization of MMA with AIBN, and model predictions were made, using the equations of the extruder. The REX model was then modified to conduct simulations in an isothermal way by setting a constant temperature. Polymerizations at several temperatures and at two different initiator concentrations were used. The experimental data consisted of conversion versus time, as well as number-average and weight-average molecular weight measurements.

Figure 10 shows experimental data and model predictions at 70 °C and 0.5 wt % of azo-bis-isobutyronitrile (AIBN) ($f = 0.6$). The agreement is very good. Figure 11 shows experimental data and the predicted profile of number-average molecular weight M_n against conversion X. Although the model predictions are higher at low and intermediate conversions, and a sharper decrease is predicted at higher conversions, the agreement is quite good. The overprediction on the number-average molecular weight calculations at low and intermediate conversions may be caused by a possibly inaccurate estimate of the free-volume parameter A (which represents the auto-acceleration effect), because the relationship between k_{tw} and polydispersity, given by eq 27, is of an approximate nature. The parameter estimation procedure that was performed by Vivaldo-Lima et al.[34] used conversion and weight-average molecular weight as responses; therefore, the value might have been slightly overestimated, to provide a good fit in M_w, causing a slight overprediction in M_n at low and intermediate conversions.

Figure 12 shows a comparison between experimental data and the predicted profile calculated with the model of weight-average molecular weight M_w under the same conditions of Figures 10 and 11. Very good agreement is observed at low and intermediate conversions, and an apparent mismatch is observed at high conversions. However, the repeats in the plot indicate that the experimental error is rather high, and the model predictions lie within the experimental data. It is also possible that the sudden decrease in M_n and M_w at ~80% of monomer conversion may be caused by the fact of modeling the glassy effect (diffusion-controlled propaga-

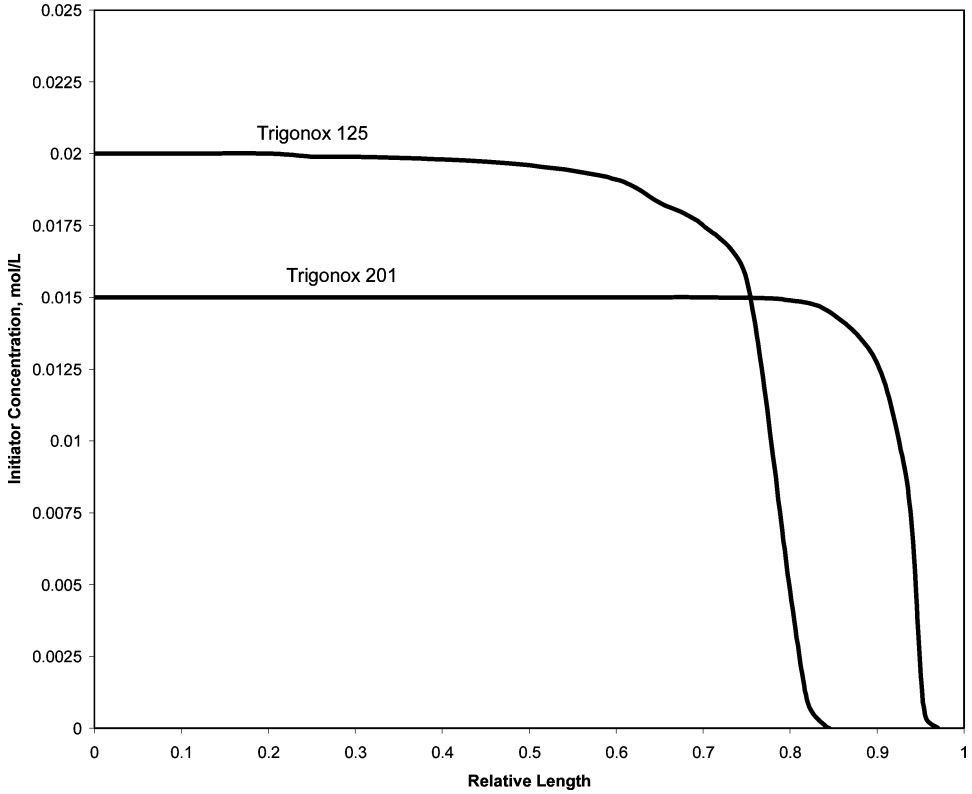

Figure 5. Calculated profiles of the initiators used in the process formulation (Trigonox 125 and Trigonox 201), under the conditions of Table 4.

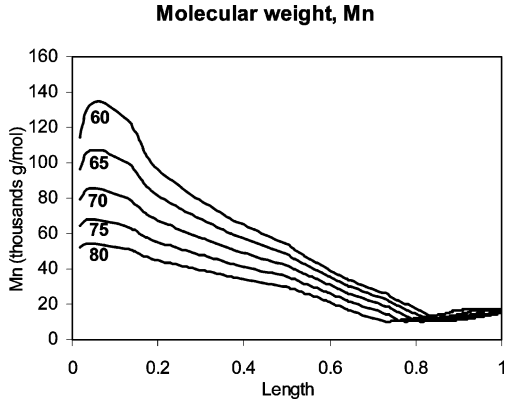

Figure 6. Effect of the feed temperature (60, 65, 70, 75, and 80 °C) on the number-average molecular weight versus fractional extruder length.

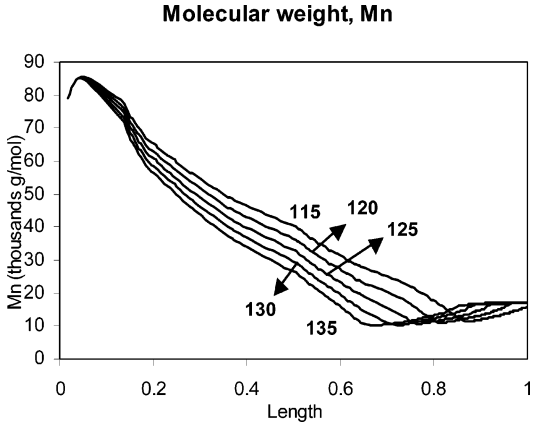

Figure 7. Effect of barrel temperature (115, 120, 125, 130, and 135 °C) on the number-average molecular weight versus fractional extruder length.

tion) using a discontinuous equation, and not considering the reaction−diffusion or residual termination, which is important and, indeed, is the dominant termination mechanism at high conversions.[26,34] If the residual termination had been considered, M_w would have experienced a slightly greater increase, in a less abrupt way, thus showing better agreement with the experimental data at high conversions. It is interesting to note that simulation studies for free-radical polymerization using models based on solving the kinetic and moment equations (e.g., Vivaldo-Lima and co-workers[26,34]) show results that are very similar to those obtained here.

Concluding Remarks

The heat of reaction strongly determines the temperature of the reaction mixture, which, in turn, has a strong influence on the viscosity. The viscosity of the reaction mixture is dependent largely on the rotational speed of the screw and other processing/operational variables, such as polymer concentration and temperature. The viscosity profiles obtained in these simulations reflect the drastic decrease in molecular weight along the extruder length caused by the exceptional increase in temperature, on one hand, and the relative increase due to polymer concentration, on the other hand. Thus, the control of operation variables is a very important feature if adequate product properties are sought.

It is important to note that, although the calculations performed in this paper, under the reported process conditions and model parameters, predict very high temperature values along the extruder length (and, thus, very low molecular weights), that does not mean that such process conditions are recommended for real application. As a matter of fact, the production of such a low molecular weight in the extruder should be

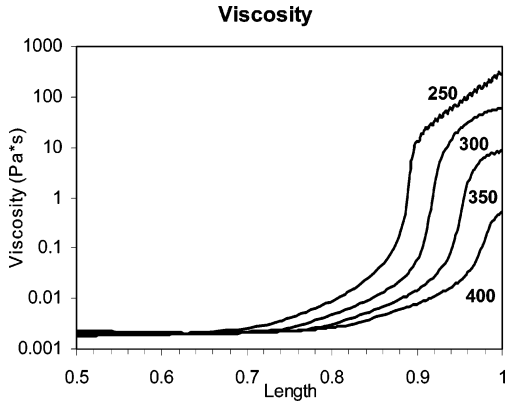

Figure 8. Viscosity versus fractional extruder length for feed mass flow rates of 15.77, 18.93, 22.08, and 25.23 L/s (250, 300, 350, and 400 gal/min).

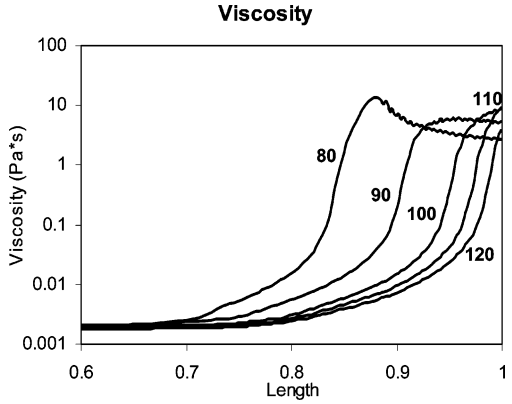

Figure 9. Viscosity versus fractional extruder length for screw rotational speeds of 8.38−12.57 rad/s (80−120 rpm).

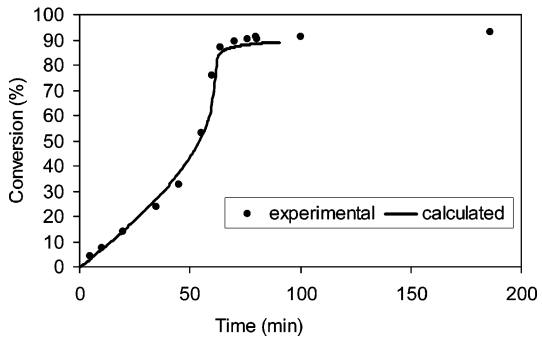

Figure 10. Comparison of experimental data[41] and the calculated profile of conversion versus (residence) time, for a reaction performed at 70 °C and using 0.5 wt % of initiator.

avoided by choosing the operation variables and feed conditions properly, as well as the exit temperature. Future research in this area should provide abundant experimental data, from which reliable model parameters can be estimated. Once that is accomplished, further studies on the design and optimization of co-rotating twin-screw extruders for methyl methacrylate (MMA) polymerization will be possible.

The feed temperature and the barrel temperature influence the number-average and weight-average molecular weights along the extruder length. The feed temperature is an important variable in the early stages, and the barrel temperature is also important in the latter stages. Generally, the increase in the screw speed decreases the residence time but increases the

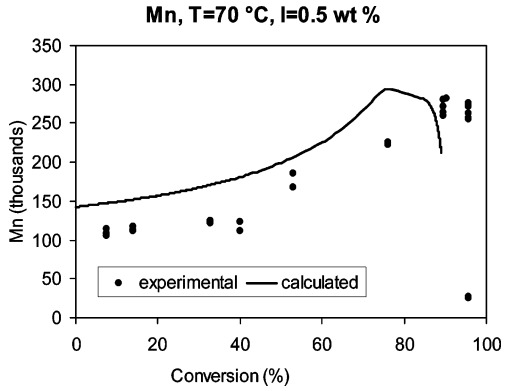

Figure 11. Comparison of experimental data[41] and the calculated profile of the number-average molecular weight (M_n) versus conversion, for a reaction performed at 70 °C and using 0.5 wt % of initiator.

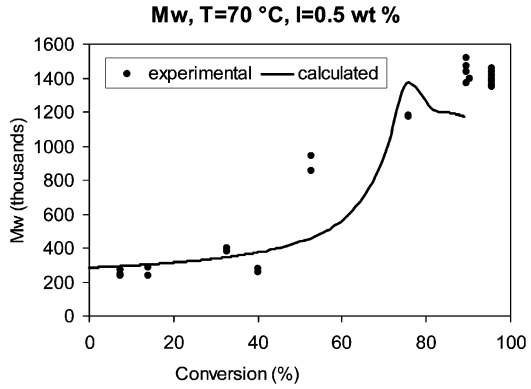

Figure 12. Comparison of experimental data[41] and calculated profiles of the weight-average molecular weight (M_w) versus conversion, for a reaction performed at 70 °C and using 0.5 wt % of initiator.

product temperature, because of higher viscous dissipation. This is observed in Figure 9, where, despite the reduction in residence time by increasing the rotational speed, the viscosity is lower at higher speeds. This reflects the loss of molecular weight, because the temperature is higher at higher screw speeds.

The mathematical equations used here to model flow in a co-rotating twin-screw extruder are an oversimplified approach to the real non-Newtonian behavior inside a real extruder. However, the main trends and observations on the effects of configuration, operational, and formulation variables on residence time, viscosity, conversion, molecular weight development, and temperature profiles inside the extruder are adequately captured.

The rigorous approach to model an extruder requires solution of the local equations of motion, energy, and mass, coupled with the polymerization kinetics and model equations along the extruder length. This would be an extremely difficult model to solve, even if three-dimensional computational fluid dynamics simulation packages were used.

An important aspect to consider if the model was to be used with semiquantitative purposes, is that the kinetic rate constants for the different reactions involved in the polymerization were obtained from experimental studies at moderately low temperatures (<373 K), and the usual temperatures inside a extruder are well above that upper limit.

Acknowledgment

The authors acknowledge financial support from CONACYT, through Projects G27837-U and U40259-Y, and DGAPA-UNAM, Project PAPIIT IN106302. The authors are grateful to the researchers of CID, R&D DESC Chemical Sector (formerly GIRSA), for the exchange of ideas and the use of their facilities.

Nomenclature

A = overlap factor in diffusion-controlled termination (autoacceleration effect)
B = overlap factor in diffusion-controlled propagation (dimensionless) or screw pitch (cm)
B_e = equivalent pitch for kneading disks (cm)
C_L = centerline distance (cm)
C_p = specific heat capacity at constant pressure (kJ kg^{-1} K^{-1})
D = overlap factor for diffusion-controlled initiation
D_n = dead polymer chain of size n
e = flight thickness (cm)
f = initiator efficiency
fr = filling ratio
f_0 = initiator initial efficiency
F_d = shape factor for the drag term
F_p = shape factor for the pressure term
F_{pl} = shape factor for leakage flow in the kneading disks
h_e = equivalent depth for kneading disks (cm)
h_{el} = equivalent depth for leakage channel of kneading disks (cm)
h_{Tb} = barrel heat-transfer coefficient (W m^{-2} K^{-1})
h_{Ts} = screw heat-transfer coefficient (W m^{-2} K^{-1})
H_p = heat of polymerization (kJ/mol)
I_i = molecule of initiator i (i = 1, 2, ..., 5), or initiator concentration (mol/L)
k_{di} = kinetic rate constant for initiator i decomposition (i = 1, 2, ..., 5) (s^{-1})
k_i = propagation kinetic rate constant for primary radicals, to produce a radical of length l (L mol^{-1} s^{-1})
k_{it} = kinetic rate constant for thermal initiation (L mol^{-1} s^{-1})
k_p = propagation kinetic rate constant (L mol^{-1} s^{-1})
k_{p0} = propagation kinetic rate constant, under initial conditions (L mol^{-1} s^{-1})
k_{tc} = termination by combination kinetic rate constant (L mol^{-1} s^{-1})
k_{td} = termination by disproportionation kinetic rate constant (L mol^{-1} s^{-1})
k_{t0} = overall termination kinetic rate constant, under initial conditions (L mol^{-1} s^{-1})
k_{tn} = number-average termination kinetic rate constant (L mol^{-1} s^{-1})
k_{tw} = weight-average termination kinetic rate constant (L mol^{-1} s^{-1})
L = length in the z-direction (cm)
L_{el} = equivalent length for channel leakage in kneading disks (cm)
m = number of parallel screw channels
m' = Ellis constant
M_n = number-average molecular weight (g/mol)
M_w = weight-average molecular weight (g/mol)
n = power-law constant
N = screw rotational speed (rad/s)
P_C = pressure in a C-shaped chamber (bar)
P_l = pressure of the channel leakage in the kneading disks (bar)
P_n = live polymer chain of size n
$\overline{P_n}$ = accumulated number-average chain length
$\overline{P_w}$ = accumulated weight-average chain length
Q_C = flow through a C-shaped chamber (cm^3/s)
Q_f = overflight flow (cm^3/s)
Q_L = leakage flow in kneading disks (cm^3/s)
r = radius (cm)
R^* = total free-radical concentration (mol/L)
R_e = screw external radius (cm)
R_i = screw internal radius (cm)
R_p = polymerization rate (mol L^{-1} s^{-1})
R_X = rate law expression for species X (where X = I, M, λ_0, λ_1, λ_2, μ_0, μ_1, and μ_2, for the initiator, monomer, zeroth, first, and second moments of the polymer radical population, and the zeroth, first, and second moments of the dead polymer population, respectively) (mol L^{-1} s^{-1})
S_b = heat-exchange surface for the barrel (cm^2)
S_s = heat-exchange surface for the screw (cm^2)
t_s = residence time (min)
T = temperature (°C)
T_b = barrel temperature (°C)
T_s = screw temperature (°C)
T_{gx} = glass-transition temperature of species x (x = polymer or monomer) (°C)
V = available free volume of a screw element (cm^3), or reaction volume (L)
$\bar{V}$ = mean barrel velocity along the channel direction (cm/s)
V_e = relative barrel velocity in the angular direction (cm/s)
V_f = fractional free volume
V_{f_0} = initial fractional free volume (at zero conversion)
$V_{f_{cr2}}$ = fractional free volume for the "glass effect"
w = axial component of velocity across the C-shaped chamber (cm/s)
W = channel width (cm)
W^* = width of the intermeshing area (cm)
$\dot{W}$ = dissipated power (W)
We = barrel relative velocity in the axial direction (cm/s)
W_e = equivalent width for kneading disks (cm)
W_{el} = equivalent width for leakage channel in kneading disks (cm)
X = conversion

Greek Letters

α = kneading disk tip angle (degrees)
α_i = volumetric expansion coefficient for species i (°C^{-1})
$\dot{\gamma}$ = shear rate (s^{-1})
$\Delta\theta_C$ = angle of a C-shaped chamber (degrees)
$\Delta\theta_l$ = staggering angle of two adjacent kneading disks (degrees)
ϕ = screw pitch angle (degrees)
ϕ_e = equivalent angle for kneading disks (degrees)
η = viscosity (Pa·s)
η_0 = zero shear viscosity (Pa·s)
λ_i = moments of the live polymer radical distribution (mol/L)
μ_i = moments of the dead polymer radical distribution (mol/L)
v = angular velocity component along the C-shaped chamber (cm/s)
ρ = density (g/cm^3)
ψ = angle of the screw intersection zone (from ref 23)
Ω = screw rotation speed (rad/s)

Literature Cited

(1) Janssen, L. P. B. M. *Twin Screw Extrusion*; Elsevier Science Publishers: Amsterdam, 1978.

(2) Vergnes, B.; Della Valle, G.; Delamare, L. A Global Computer Software for Polymer Flows in Corotating Twin Screw Extruders. *Polym. Eng. Sci.* **1998**, *38*, 1781−1792.

(3) White, J. L.; Szydlowski, W. Composite Models of Modular Intermeshing Corotating and Tangential Counter-Rotating Twin Screw Extruders. *Adv. Polym. Technol.* **1987**, *7*, 419.

(4) Wang, Y.; White, J. L.; Szydlowski, W. Non-Newtonian Flow Modeling and Experimental Studies of Flow in a Modular Intermeshing Co-Rotating Twin Screw Extruder. *Int. Polym. Process.* **1989**, *4*, 262.

(5) Szydlowski, W.; White, J. L. Improved Theory of Metering in an Intermeshing Co-Rotating Twin-Screw Extruder. *Adv. Polym. Technol.* **1987**, *7*, 177.

(6) Wang, Y.; White, J. L. Non-Newtonian Flow Modeling in the Screw Regions of an Intermeshing Corotating Twin Screw Extruder. *J. Non-Newtonian Fluid Mech.* **1989**, *32*, 19.

(7) Meijer, H. E. H.; Elemans, P. M. Modeling of Contiuous Mixers. Part I: The Corotating Twin-Screw Extruder. *Polym. Eng. Sci.* **1988**, *28*, 275.

(8) Chen, Z.; White, J. L. Simulation of Nonisothermal Flow in Twin Screw Extrusion. *Int. Polym. Process.* **1994**, *9*, 310.

(9) White, J. L.; Chen, Z. Simulation of nonisothermal flow in modular co-rotating twin screw extrusion. *Polym. Eng. Sci*. **1994**, *34*, 229.

(10) Potente, H.; Ansahl, J.; Klarholz, B. Design of Tightly Intermeshing Co-Rotating Twin Screw Extruders. *Int. Polym. Process*. **1994**, *9*, 11.

(11) Potente, H.; Melisch, U.; Flecke, J. SIGMA−computer aided process simulation of intermeshing co-rotating twin-screw extruders. *SPE Annu. Tech. Conf. Proc.* **1996**, *42*, 334.

(12) Berzin, F.; Vergnes, B. Transesterification of ethylene acetate copolymer in a twin screw extruder—Experimental and theoretical approaches. *Int. Polym. Process.* **1998**, *13*, 13−22.

(13) Berzin, F.; Vergnes, B.; Dufosse, P.; Delamare, L. Modeling of peroxide initiated controlled degradation of polypropylene in a twin screw extruder. *Polym. Eng. Sci.* **2000**, *40*, 344−356.

(14) Fukuoka, T. Numerical analysis of a reactive extrusion process. Part II: Simulations and verifications for the twin screw extrusion. *Polym. Eng. Sci.* **2000**, *40* (12), 2524−2538.

(15) Janssen, L. P. B. M.; Rozendal, P. F.; Hoogstraten, H. W.; Cioffi, M. A dynamic model for multiple steady states in reactive extrusion. *Int. Polym. Process.* **2001**, *16* (3), 263−271.

(16) Gaspar-Cunha, A.; Poulesquen, A.; Vergnes, B.; Covas, J. A. Optimization of processing conditions for polymer twin-screw extrusion. *Int. Polym. Process.* **2002**, *17* (3), 201−213.

(17) Poulesquen, A.; Vergnes, B. A study of residence time distribution in co-rotating twin-screw extruders. Part I. Theoretical modeling. *Polym. Eng. Sci.* **2003**, *43* (12), 1841−1848.

(18) Gao, S. S.; Ying, Z.; Anna, Z.; Xia, H. N. Polystyrene prepared by reactive extrusion: kinetics and effect of processing parameters. *Polym. Adv. Technol.* **2004**, *15* (4), 185−191.

(19) Choulak, S.; Couenne, F.; Le Gorrec, Y.; Jallut, C.; Cassagnau, P.; Michel, A. Generic dynamic model for simulation and control of reactive extrusion. *Ind. Eng. Chem. Res.* **2004**, *43* (23), 7373−7382.

(20) Vergnes, B.; Barres, C.; Tayeb, J. Computation of Residence Time and Energy Distributions in the Reverse Screw Element of a Twin-Screw Extrusion-Cooker. *J. Food Eng.* **1992**, *16*, 215.

(21) Tayeb, J.; Vergnes, B.; Della Valle, G. Theoretical Computation of the Isothermal Flow Through the Reverse Screw Element of a Twin Screw Extrusion Cooker. *J. Food Sci.* **1988**, *53*, 616.

(22) Tayeb, J.; Vergnes, B.; Della Valle, G. A Basic Model for a Twin-Screw Extruder. *J. Food Sci.* **1988**, *53*, 1047.

(23) Booy, M. L. Geometry of Fully Wiped Twin-Screw Equipment. *Polym. Eng. Sci.* **1978**, *18*, 973.

(24) Della Valle, G.; Barres, C.; Plewa, J.; Tayeb, J.; Vergnes, B. Computer Simulation of Starchy Products, Transformation by Twin-Screw Extrusion. *J. Food Eng.* **1993**, *19*, 1.

(25) Stuber, N. P. Studies of Continuous Methyl Methacrylate Polymerization in a Twin-Screw Extruder, Ph.D. Thesis, University of Minnesota, Minneapolis, MN, 1986.

(26) Vivaldo-Lima, E.; Hamielec, A. E.; Wood, P. E. Auto-Acceleration Effect in Free Radical Polimerization. A Comparison of the CCS and MH Models. *Polym. React. Eng.* **1994**, *2* (1&2), 17−86.

(27) Marten, F. L.; Hamielec, A. E. High conversion diffusion controlled polymerization of styrene. *J. Appl. Polym. Sci*. **1982**, *27*, 489.

(28) Chiu, W. Y.; Carrat, G. M.; Soong, D. S. A Computer Model for the Gel Effect in Free-Radical Polymerization. *Macromolecules* **1983**, *16*, 348.

(29) Zhu, S.; Hamielec, A. E. Chain-Length-Dependent Termination for Free Radical Polymerization. *Macromolecules* **1989**, *22*, 3093.

(30) Todd, D. B. *SPE Annu. Tech. Conf. Proc.* **1988**, *34*, 54.

(31) Keum, J.; White, J. L. Simulations of Grafting Monomers and Associated Degradation of Polypropylene in a Modular Co−Rotating Twin Screw Extruder. *SPE Annu. Tech. Conf. Proc.* **2005**, 3367−3371.

(32) Bawiskar, S.; White, J. L. *Int. Polym. Process.* **1997**, *12*, 331.

(33) White, J. L.; Kim, B. J.; Bawiskar, S.; Keum, J. *Polym. Plast. Technol. Eng.* **2001**, *40*, 385.

(34) Vivaldo-Lima, E.; García-Pérez, R.; Celedón-Briones, O. J. Modeling of the Free-Radical Copolymerization Kinetics with Cross-linking of Methyl Methacrylate/Ethylene Glycol Dimethacrylate Up to High Conversions and Considering Thermal Effects. *Rev. Soc. Quím. Mex.* **2003**, *47* (1), 22−33.

(35) Wunderlich, W. Physical Constants of Poly(methyl methacrylate). In *Polymer Handbook*; Brandrup, J., Immergut, E. H., Grulke, E. A., Eds.; Wiley: New York, 1999; p V/87.

(36) Akzo Nobel Chemicals, Inc. *Initiators for Polymer Production Product Catalog*; Publication PC-2002-05-b, 2002 (web site: http://www.akzonobel-polymerchemicals.com/ProductGroups/Brochures+for+Polymerization+Initiators.htm).

(37) Guerrero Sánchez, C. A. *Modelamiento y Simulació*n de Sistemas de Copolimerización por Radicales Libres, Casos: Masa y Emulsión, B. Sc. Thesis in Chemical Engineering, Universidad Nacional Autónoma de México (UNAM), Mexico D.F., 1999.

(38) Beuermann, S.; Buback, M.; Davis, T. P.; Gilbert, R. G.; Hutchinson, R. A.; Olaj, O. F.; Russell, G. T.; Schweer, J.; van Herk, A. M. Critically evaluated rate coefficients for free-radical polymerization, 2. Propagation rate coefficients for methyl methacrylate. *Macromol. Chem. Phys.* **1997**, *198* (5), 1545−1560.

(39) Hutchinson, R. A. Modeling of free-radical polymerization kinetics with cross-linking for methyl methacrylate/ethylene glycol dimethacrylate. *Polym. React. Eng.* **1992−1993**, *1* (4), 521−277.

(40) Tulig, T. J.; Tirrel, M. On the Onset of the Trommsdorff Effect. *Macromolecules* **1982**, *15*, 459.

(41) Balke, S. T.; Hamielec, A. E. Bulk Polymerization of Methyl Methacrylate. *J. Appl. Polym. Sci.* **1973**, *17*, 905.

Received for review May 17, 2005
Revised manuscript received September 4, 2005
Accepted October 4, 2005

IE050585B